Relative energetics and structural properties of zirconia using a self-consistent tight-binding model

Stefano Fabris, Anthony T. Paxton, and Michael W. Finnis
Atomistic Simulation Group, Department of Pure and Applied Physics, Queen's University, Belfast BT7 1NN, United Kingdom
(Received 31 August 1999)

We describe an empirical, self-consistent, orthogonal tight-binding model for zirconia, which allows for the polarizability of the anions at dipole and quadrupole levels and for crystal field splitting of the cation *d* orbitals. This is achieved by mixing the orbitals of different symmetry on a site with coupling coefficients driven by the Coulomb potentials up to octapole level. The additional forces on atoms due to the self-consistency and polarizabilities are exactly obtained by straightforward electrostatics, by analogy with the Hellmann-Feynman theorem as applied in first-principles calculations. The model correctly orders the zero temperature energies of all zirconia polymorphs. The Zr-O matrix elements of the Hamiltonian, which measure covalency, make a greater contribution than the polarizability to the energy differences between phases. Results for elastic constants of the cubic and tetragonal phases and phonon frequencies of the cubic phase are also presented and compared with some experimental data and first-principles calculations. We suggest that the model will be useful for studying finite temperature effects by means of molecular dynamics.

I. INTRODUCTION

Solid solutions of zirconia (ZrO_2) containing other oxides are among the major representatives of modern ceramic materials. The wide range of applications, including traditional structural refractories, fuel cells, and electronic devices such as oxygen sensors,[1,2] testifies to the technological importance of zirconias. Different divalent and trivalent oxides are added to ZrO_2 in order to improve its thermomechanical properties, and charge-compensating vacancies are thereby introduced on the anion sublattice. The macroscopic effects associated with the impurities are very well known,[3–5] but a microscopic model that gives a theoretical interpretation is still missing. As a preliminary step, this paper provides a physical picture of the crystal thermodynamics of pure zirconia, combining the results of first-principles density functional and semiempirical Tight Binding (TB) calculations.

Zirconia has three zero-pressure polymorphs; these have cubic (c), tetragonal (t), and monoclinic (m) symmetry. The high-temperature c phase[6,7] ($Fm3m$) is stable between 2570 K and the melting temperature of 2980 K. The t structure[8,9] ($P4_2/nmc$), which is stable between 1400 and 2570 K, is closely related to the c one: the internal degree of freedom δ shifts the oxygen ions away from the centrosymmetric positions along the X_2^- mode of vibration (Fig. 1) and forces the c/a ratio of the unit cell to adjust. Below 1400 K the low-symmetry m phase[10–12] ($P2_1/c$) is thermodynamically stable.

Besides its technological implications, the relationship between these structures is of fundamental interest. The mechanisms of the phase transformations, the effects of impurities and vacancies on them, and their relationship to the nature of the bonding still require explanation, and this may shed light on the properties of other, more complex oxides.

The crystal structure of purely ionic bonded materials can be determined on the basis of radius-ratio rules,[13] based purely on electrostatic arguments. Because of the small size of the Zr^{4+} ions, these rules place ZrO_2 on the border between the eightfold coordinated fluorite structure and the sixfold coordinated rutile one ($P4_2/mnm$). The radius-ratio is too blunt a tool to account for the absolute stability of the unique sevenfold coordinated m structure.

The classical empirical models of zirconia are based on the *a priori* assumption of its *ionicity*. Empirical approaches like the shell model or the rigid ion model (RIM) described the structural,[14] dynamical,[15,16] and transport[17–19] properties of the phases on which they were parameterized, but failed to predict the absolute stability of the m structure. The most detailed of such models was developed by Wilson *et al.*,[20] whose environment-dependent compressible and polarizable ion model (CIM-DQ) demonstrated the importance of the anion polarizabilities at both dipole and quadrupole levels on

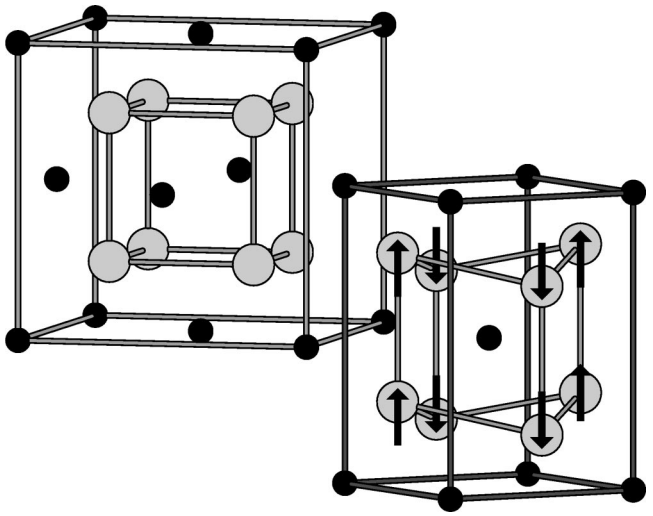

FIG. 1. Cubic and tetragonal structures of ZrO_2. Light and dark circles denote oxygen and zirconium atoms, respectively. Arrows represent the structural instability of the oxygen sublattice along the X_2^- mode of vibration.

the energetics of zirconia. However, further calculations[21] carried out with this model revealed that even though it predicted the correct energy ordering of the *c*, *t*, and *m* phases, it predicted that the rutile structure should be even more stable, and this phase is never observed experimentally in zirconia.

The experience gained with the CIM-DQ model suggests that a successful empirical model of zirconia should describe the effects of the atomic polarization, but should also go beyond a purely ionic description of the bonding. The partial covalent character of zirconia has already been postulated[22] and is evident from electronic structure calculations based on density functional theory. In this paper we further investigate the recently proposed polarizable self-consistent tight binding (SC-TB) model,[23–25] which combines the physical concepts of covalency, ionicity, and polarizability. Using the SC-TB model we are drawn to the conclusion that the covalent character of the Zr-O bond makes a significant contribution to the relative energetics of different structures, which would explain the limited predictive power of the previous ionic models.

There have been several previous approaches to analyzing the structural and electronic properties of zirconia. Boyer and Klein[26] used the augmented plane wave (APW) method to derive pair potentials with which to investigate the equation of state of the *c* phase. Cohen *et al.*[27] calculated the relative energetics and the elasticity using the Potential Induced Breathing (PIB) method based on the Gordon-Kim approach. Zandiehnadem *et al.*[28] studied the electronic structure with a first-principles linear combination of atomic orbitals method. The FLAPW calculations of Jansen[29] predicted for the first time the correct energetic ordering between the *c* and *t* structures at zero absolute temperature, identifying the double well in the potential energy that governs their relative stability. The double well was subsequently confirmed by *ab initio* Hartree-Fock (HF) calculations,[30,31] but these did not predict the stability of the *m* structure over the *t* one. Only the very recent density functional theory (DFT) calculations[32–34] consistently reproduce the relative energetics of the three zirconia polymorphs at 0 K.

The plan of the present paper is as follows. In Sec. II we describe the model used in the calculations, the inclusion of the atomic polarizability in the TB framework and the parametrization procedure. A preliminary account of this work has been published.[24] We have made DFT calculations of band structures of the simple structures for this purpose, using a new full-potential, linear muffin tin orbital method (NFP-LMTO). The predictive power of the new model is tested against the DFT calculations in Sec. III A, where we study the relative energetics of zirconia. Section III B focuses on the relationship between the *c* and *t* structures: the Landau theory of phase transformation is used to interpret the results of the static calculations. In Sec. IV, we explore the elastic and the vibrational properties of the high symmetry phases. The results are summarized in the concluding section.

II. THE TIGHT-BINDING MODEL

A. Including polarizabilities in TB

In the TB approximation the crystal wave function can be expressed as a linear combination of atom-centred orbitals, which we denote $|\mathbf{R}L\rangle$:

$$|\Psi^{n\mathbf{k}}\rangle = \sum_{\mathbf{R}l} c^{n\mathbf{k}}_{\mathbf{R}L} |\mathbf{R}L\rangle. \tag{1}$$

L is a composite angular momentum index $L=(l,m)$ of the atomic orbital centered on the site whose position is $\mathbf{R}$, n and $\mathbf{k}$ are the band and $\mathbf{k}$-vector indices of the single particle wave function. For the purpose of derivation, we express the local orbitals as a product of a radial function and a real spherical harmonic

$$\langle \mathbf{r}|\mathbf{R}L\rangle = f_{\mathbf{R}l}(|\mathbf{r}-\mathbf{R}|)Y_L(\mathbf{r}-\mathbf{R}), \tag{2}$$

although in our *empirical* TB scheme the explicit functional forms of the radial wave functions are not required. To simplify the notation, we will frequently suppress the site index $\mathbf{R}$, in which case one can take it we are referring to an atom at the origin and $\mathbf{r}$ is a small vector in its neighborhood.

The total Hamiltonian $\mathcal{H}$ can be expressed as a sum of two terms, $\mathcal{H}=\mathcal{H}^0+\mathcal{H}'$. In traditional self-consistent (SC) TB, $\mathcal{H}^0$ contains both on-site and intersite terms. The on-site terms are diagonal in L, and are often taken as Hartree-Fock term values of the isolated atoms. The intersite terms are the bonding integrals. The additional part of the Hamiltonian, $\mathcal{H}'$, is diagonal in $\mathbf{R}$ and L in the traditional approach (Majewski and Vogl[35,36]). It controls the charge redistribution between neighboring sites, which results from the balance between the opposite effects due to the on-site Coulomb repulsion (Hubbard U) and Madelung potentials.

What is missing in the previous model is the effect of the crystal fields on the valence electrons, i.e., the atomic *polarizability*. In a preliminary account of this work[24] we indicated how to include the polarization effects in a SC-TB formalism by adding off-diagonal terms $\mathcal{H}'_{\mathbf{R}L\mathbf{R}L'}$ to the on-site blocks of the Hamiltonian. Here we describe how we make that extension.

If we assume the on-site charge distribution to be localized, then its total multipole moment Q_L has a monopole contribution from the ionic core charge and a multipole (including monopole) contribution from the valence charge:

$$Q_L = Q^i \delta_{L0} + Q^e_L. \tag{3}$$

As Stone[37] points out, the electronic multipole moment on a site is the expectation value of the operator

$$\hat{Q}^e_L = e\hat{r}^l Y_L(\hat{\mathbf{r}}), \tag{4}$$

where e is the charge of the electron. Neglecting intersite terms like $\langle \mathbf{R}'L'|\hat{Q}^e_{\mathbf{R}L}|\mathbf{R}''L''\rangle$ for $\mathbf{R}',\mathbf{R}''\neq\mathbf{R}$, the definition of the on-site multipole moment is therefore

$$Q^e_L \equiv \sum_{L'L''} \sum_{n\mathbf{k}}^{\text{occ.}} c^{n\mathbf{k}}_{L'} c^{n\mathbf{k}}_{L''} \langle L'|\hat{Q}^e_L|L''\rangle. \tag{5}$$

By invoking equations (2) and (4), the last factor of Eq. (5) can be expressed as a product of two quantities, the Gaunt coefficients $C_{L'L''L}$, which dictate the selection rules, and the integrals $\Delta_{l'l''l}$, which will be new parameters of the model:

$$\langle L'|\hat{Q}^e_L|L''\rangle = e\,\Delta_{l'l''l}\,C_{L'L''L}, \tag{6}$$

$$C_{L'L''L} = \int Y_{L'} Y_{L''} Y_L d\Omega, \tag{7}$$

$$\Delta_{l'l''l} = \int f_{l'}(r) f_{l''}(r) r^{l+2} dr, \tag{8}$$

where $d\Omega$ stands for the element of solid angle $\sin\theta d\theta d\phi$. The role of the Gaunt coefficients, which depend on the angular part of the wave function only, is to select the term with symmetry L arising from the coupling of the on-site orbitals L' and L''. The Δ parameters, depending on the radial part of the wave function, determine the magnitude of the coupling. The substitution of Eq. (6) in Eq. (5) defines the multipole moment of symmetry L on the site $\mathbf{R}$.

Having defined the on-site multipole moments, we can calculate the fields that they generate on all the lattice sites. The derivation uses standard results from classical electrostatics. The electrostatic potential is expanded in partial waves about the site:

$$V(\mathbf{r}) = \sum_L V_L r^l Y_L(\mathbf{r}), \tag{9}$$

where, using the Poisson equation,

$$V_L = 4\pi \sum_{\mathbf{R}' \neq \mathbf{0}} \sum_{L'} \tilde{B}_{LL'}(\mathbf{R}') Q_{\mathbf{R}'L'}, \tag{10}$$

and

$$\tilde{B}_{LL'}(\mathbf{R}) = \frac{4\pi}{(2l+1)!!(2l'+1)!!} \times \sum_{L''} \frac{(-1)^{l'}(2l''-1)!!}{|\mathbf{R}|^{l''+1}} Y_{L''}(\mathbf{R}) C_{L''L'L}. \tag{11}$$

The sum over L'' is restricted to the values for which $l'' = l + l'$; $\tilde{B}_{LL'}$ are proportional to the well-known LMTO-ASA structure constants.[38] The component of electrostatic potential V_L couples different orbitals on a site giving the matrix elements:

$$\langle L' | \mathcal{H}' | L'' \rangle = \sum_L V_L \Delta_{l'l''l} C_{L'L''L}. \tag{12}$$

The diagonal elements of the Hamiltonian are adjusted by using a single Hubbard U in the standard way, which adds a term $U\delta N_{\mathbf{R}l}$ to each diagonal matrix element. The quantities $\delta N_{\mathbf{R}l}$ are the changes in the electronic charge projected onto a site and orbital compared to the input, non-self-consistent charge. We use the standard Mulliken projection. Finally the Schrödinger equation is solved using a self-consistent iterative procedure with charge mixing to obtain the coefficients $c^{n\mathbf{k}}_{\mathbf{R}L}$ and hence the multipoles.

It is useful to step back at this point and compare the above model with the Hohenberg-Kohn-Sham one, whose exchange and correlation energy functional $U^{xc}[n]$ has been expanded to second order in the electron density n($\mathbf{r}$):[39]

$$U^{\mathrm{HKS}} = \sum_{n,\mathbf{k}}^{\mathrm{occ}} \langle \Psi^{n\mathbf{k}} | \mathcal{T}_S + V_0^{xc} + V_0^{\mathrm{H}} + V_0^i | \Psi^{n\mathbf{k}} \rangle + U^{xc}[n_0] - \int V_0^{xc} n_0 d\mathbf{r} - U^{\mathrm{H}}[n_0] + U^{ii} + \frac{1}{2} \int \int \left(\frac{e^2}{|\mathbf{r}-\mathbf{r}'|} + \left. \frac{\delta^2 U^{xc}}{\delta n \, \delta n'} \right|_{n=n_0} \right) \delta n \, \delta n' \, d\mathbf{r} \, d\mathbf{r}'. \tag{13}$$

n_0 denotes a reference electron density, which we will consider as a superposition of spherical ionic charges; $\mathcal{T}_S$ is the kinetic energy operator of the noninteracting electron gas, V_0^{xc}, V_0^{H}, and V_0^i are the exchange and correlation, Hartree and ionic potentials calculated at the reference charge n_0; δn denotes the deviation from that reference ($\delta n = n - n_0$) and n' refers to the electron density at $\mathbf{r}'$. U^{H} and U^{ii} are, respectively, the Hartree and the ion-ion electrostatic energies.

Without the last term, this is simply the Harris-Foulkes functional. It generates a non-self-consistent TB model in which the first term is the sum of the eigenvalues while the second is a sum of pair potentials.[40] If the last term is included, the total energy must be minimized iteratively, and the last term now provides the self-consistency correction to the Kohn-Sham Hamiltonian.

The last line of Eq. (13) represents the Hartree energy of the deviation from the reference charge, $U^{\mathrm{H}}[\delta n]$, and the second-order term of the U^{xc} Taylor expansion. We can identify this term in our SC-TB model as follows:

$$\frac{1}{2} \int \int \left(\frac{e^2}{|\mathbf{r}-\mathbf{r}'|} + \left. \frac{\delta^2 U^{xc}}{\delta n \, \delta n'} \right|_{n=n_0} \right) \delta n \, \delta n' \, d\mathbf{r} d\mathbf{r}' \equiv \frac{1}{2} \sum_{\mathbf{R}L} (U \delta N^2_{\mathbf{R}l} + Q_{\mathbf{R}L} V_{\mathbf{R}L}). \tag{14}$$

Our total energy in the SC-TB model is therefore

$$U^{\mathrm{TB}} = \sum_{n,\mathbf{k}}^{\mathrm{occ}} \langle \Psi^{n\mathbf{k}} | \mathcal{H}^0 | \Psi^{n\mathbf{k}} \rangle + U^{\mathrm{pair}} + \frac{1}{2} \sum_{\mathbf{R}L} (U \delta N^2_{\mathbf{R}l} + Q_{\mathbf{R}L} V_{\mathbf{R}L}). \tag{15}$$

It can be verified that, by minimizing the above expression with respect to the expansion coefficients in the wave functions, we recover the Schrödinger equation with the SC-TB Hamiltonian.

Calculation of the forces on the ions is very straightforward once we have the self-consistent wave functions and multipoles. For if an ion is moved a small distance $\delta\mathbf{R}$, there is no change in total electronic energy to first order in the $\delta c^{n\mathbf{k}}_{\mathbf{R}L}$. Therefore we can calculate the force due to the change in the first term of Eq. (15) by the conventional formulas, using the derivatives of the non-self-consistent Hamiltonian matrix elements (see following section). In calculating the forces due to the last term of Eq. (15) we can hold the multipoles fixed and use standard electrostatics. There is no con-

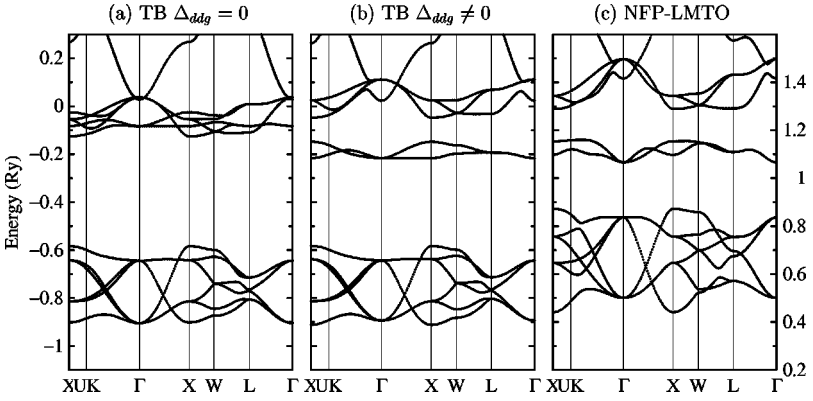

FIG. 2. Band structure of cubic zirconia. In all the panels, starting from the bottom it is possible to identify the oxygen $2p$ valence bands and the unoccupied zirconium $4d$ bands, which are partly hybridized with the oxygen $3s$ one. The large crystal field splitting of the $4d$ bands predicted by the LDA calculation (c) is reproduced with the SC-TB model, (a) and (b), when the Δ_{ddg} parameter is included.

tribution to the forces from the on-site energy containing U. The simple form of these results for the forces in TB is a direct analogy with the application of the Hellmann-Feynman theorem in DFT.

B. Parametrization

Each parameter of the model has been adjusted to the results of NFP-LMTO calculations, details of which are specified in the previous work on zirconia.[24] Our TB description of zirconia uses a minimal basis of atomic orbitals. The oxygen atoms are modeled with $2p$ and $3s$ orbitals and with a fixed core charge of $+4$, while on the zirconium atoms there are $4d$ orbitals and a core charge of $+4$. The purpose of the $3s$ orbital on the oxygen is twofold: to allow an extra degree of freedom for polarization, which is otherwise restricted to charge transfer between its $2p$ orbitals, and to better reproduce the structure of the conduction bands.

A repulsive Born-Mayer pair potential U^{pair} has been chosen in order to reproduce the lattice parameter and the bulk modulus of the c phase. Only the first Zr-O coordination shell has been included in this interaction.

The Hamiltonian $\mathcal{H}^0$ has been adjusted to the *ab initio* electronic structure of the c phase shown in Fig. 2(c). We chose the Goodwin-Skinner-Pettifor[41] distance dependence of the 10 hopping integrals involved. The Hubbard U have been fixed to 1 Ry. The parameters of the SC-TB model are collected in Table I.

The basis set chosen reduces the number of symmetry-allowed Δ parameters to 4: Δ_{spp}, Δ_{ppd}, Δ_{ddd}, and Δ_{ddg}. The first two refer to the s and p orbitals of oxygen ions, the last two to the d orbitals on the zirconium.

In the highly symmetric c structure the first nonspherical terms of the potential V_L on the cation and anion sites have g and f symmetry, respectively. The latter cannot interact with the oxygen orbitals, the former splits the energetic levels of

TABLE I. Parameters of the polarizable SC-TB model. Energy in Ry and lengths in atomic units.

On site parameters

$\mathcal{H}^0_s = 0.35$	$U_s = 1$
$\mathcal{H}^0_p = -0.70$	$U_p = 1$
$\mathcal{H}^0_d = -0.10$	$U_d = 1$

Bond integrals

$$V_{ll'}\left(\frac{d}{r}\right)^n \exp\left\{n\left[-\left(\frac{r}{r_c}\right)^{n_c}+\left(\frac{d}{r_c}\right)^{n_c}\right]\right\}$$

	$V_{ll'}$	n	n_c	d	r_c		$V_{ll'}$	n	n_c	d	r_c
$ss\sigma$	−0.060	2	0	4.90	6.24	$pd\sigma$	−0.100	4	0	4.24	4.90
$sp\sigma$	0.070	2	0	4.90	6.24	$pd\pi$	0.058	4	0	4.24	4.90
$pp\sigma$	0.050	3	4	4.90	6.24	$dd\sigma$	−0.050	5	0	6.02	6.93
$pp\pi$	−0.008	3	4	4.90	6.24	$dd\pi$	0.033	5	0	6.02	6.93
$sd\sigma$	−0.050	3	0	4.24	4.90	$dd\delta$	0.008	5	0	6.02	6.93

Polarization terms

$\Delta_{spp} = 0.73$	$\Delta_{ddd} = 0$
$\Delta_{ppd} = 1.89$	$\Delta_{ddg} = 63.5$

Pair potential

$U(r) = Ae^{(-br)}$

$A = 181.972$	$b = 1.652$

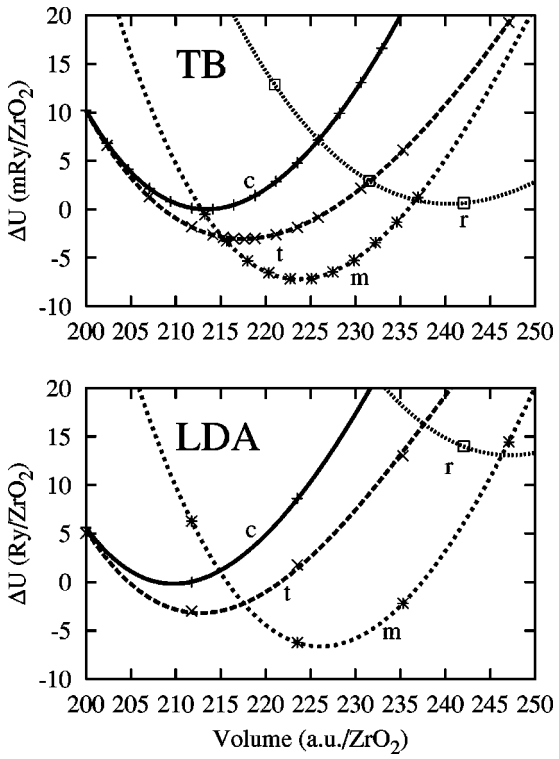

FIG. 3. SC-TB (top) and NFP-LMTO (bottom) energy-volume data for the cubic (c), tetragonal (t), monoclinic (m), and rutile (r) phases fitted with Murnaghan equation of states.

the zirconium d orbitals and Δ_{ddg} determines the magnitude of the energy splitting $\delta\epsilon$. Cubic crystal field theory[42] predicts the proportionality between $\delta\epsilon$ and the radial distribution of charge $\langle r^4 \rangle$, which is the definition of Δ_{ddg} given in Eq. (8). Figures 2(a) and 2(b) show the effect of the Δ_{ddg} polarization term on the band structure of the c phase: the splitting of the d bands could not be captured with the SC-TB without the polarizability parameters. Reasonable values of the Δ_{ddd} parameter have no significant effect on any physical properties studied here, therefore we set it to zero.

Less symmetric structures are necessary to parametrize the remaining Δ's. In the rutile phase, the $l=3$ component of the crystal field acting on the oxygen ions splits the p levels. Consequently, it contributes to the width of the $2p$ band: this effect is controlled by Δ_{ppd}, which we adjust to match the *ab initio* band structure of the rutile phase. The last term Δ_{spp} has been chosen in order to reproduce the depth of the double well in the potential energy of the t structure.

III. ENERGETICS OF BULK PHASES

A. Energy-volume curves

1. Zero-pressure phases

The predictive power of the polarizable TB model has been investigated by comparing its results with NFP-LMTO calculations. The energy-volume curves calculated with the two methods are shown in Fig. 3. Each energy value involved the full relaxation of all the degrees of freedom of the structures.

The c and the t phases were used in the parametrization procedure, therefore there is automatic agreement of the two methods for these crystal structures. The true prediction of the model is the absolute stability of the monoclinic phase. This indicates the transferability of the parameters between the phases.

The rutile phase, which is not experimentally observed, has been included in the study because further calculations with the CIM-DQ (Ref. 20) model predicted the rutile phase to be more stable than the monoclinic one. Figure 3 shows that the SC-TB model does not suffer from this problem, although the relative energy of the rutile phase is less than with the DFT. To our knowledge, the SC-TB is the first semi-empirical model, which reproduces the correct ordering of these polymorphs at zero temperature, including the stability of the m phase.

Table II summarizes the structural properties calculated with the NFP-LMTO method and with the polarizable SC-TB model, comparing them with other theoretical and experimental works. The c and m lattice parameters are referred to the 12-atom unit cell, while the t ones are given in terms of the 6-atom unit cell. A comparison of the energy differences between the phases of zirconia calculated with different methods is given in Table III.

2. High-pressure phases

Under pressure, the low temperature m phase transforms to an orthorhombic structure, known as ortho I (o_I), whose crystallography is still controversial. X-ray diffraction analysis[44,45] suggests it belongs to the $Pbcm$ space group, while neutron-diffraction studies[46,47] propose the $Pbca$ space group. We carried out the calculations using the latter structure. The phase transition pressure strongly depends on the state of the sample and is believed to be between 3 and 6 GPa.[48–50] A second pressure-induced phase transition is observed around 15 GPa,[50] where the o_I transforms to the orthorhombic phase termed ortho II (o_{II}). The latter is isostructural to cotunnite ($PbCl_2$) and belongs to the $Pnam$ space group.[51] The pressure increases the coordination number of the zirconium atoms from 7 to 9.

A comprehensive first-principles study of the two orthorhombic phases has apparently not yet been made: Stapper *et al.*[33] studied the o_I structure only, while Jomard *et al.*[34] focused on the o_{II} phase.

The atomic environment of the high-pressure phases is completely different to that of the c and t phases used in the parametrization of the TB model, therefore these orthorhombic structures provide a severe benchmark for the transferability of the TB parameters.

The energy ordering of the phases predicted by the TB model is

$$U^m < U^{o_I} < U^t < U^c < U^{o_{II}},$$

which is the same as we obtain by combining the results of Refs. 33 and 34. The numerical values of the energy differences are summarized in Table III and compare reasonably well with the *ab initio* results. The energy-volume curves of the orthorhombic phases are shown in Fig. 4: all the degrees of freedom were fully relaxed and their values are collected in Table IV.

TABLE II. Equilibrium structural parameters for the 0-pressure phases of ZrO_2. The lattice parameters a, b, c (a.u.), and the volumes (a.u./ZrO_2) of the c, t, and m structure are referred to the 12-atom, 6-atom, and 12-atom unit cells, respectively. δ denotes the internal degree of freedom of the t phase (see Fig. 1), β is the angle of the m cell in degrees, and x, y, z are the fractional coordinates of the nonequivalent sites in the m structure.

	Expt. [a] Refs. 6,8	SC-TB This work	NFP-LMTO This work	PW-PP Ref. 32	PW-PP Ref. 33	FLAPW Ref. 29
			Cubic			
Volume	222.50	213.40	210.33	215.29	220.84	217.81
a	9.619	9.486	9.442	9.514	9.595	9.551
			Tetragonal			
Volume	229.93	217.73	215.16	218.69	225.31	218.84
a	6.748	6.709	6.695	6.734	6.797	6.747
c/a	1.451	1.442	1.434	1.432	1.435	1.425
δ/c	0.057 [b]	0.047	0.051	0.042	0.042	0.029
			Monoclinic			
Volume	237.67	222.89	226.13	230.51	236.46	
a	9.733	9.592	9.417	9.611	9.733 [c]	
b/a	1.012	1.001	1.036	1.024	1.012[c]	
c/a	1.032	1.019	1.057	1.028	1.032[c]	
β	99.23	98.00	98.57	99.21	99.23[c]	
x_{Zr}	0.275	0.272	0.274	0.278	0.277	
y_{Zr}	0.040	0.027	0.040	0.042	0.043	
z_{Zr}	0.208	0.217	0.212	0.210	0.210	
x_{O_1}	0.070	0.078	0.069	0.077	0.064	
y_{O_1}	0.332	0.336	0.339	0.349	0.324	
z_{O_1}	0.345	0.342	0.338	0.331	0.352	
x_{O_2}	0.450	0.452	0.448	0.447	0.450	
y_{O_2}	0.757	0.752	0.753	0.759	0.756	
z_{O_2}	0.479	0.472	0.478	0.483	0.479	

[a]The experimental values of the cubic and tetragonal structures have been extrapolated at 0 K using the thermal expansion data from Ref. 6.
[b]At 1568 K.
[c]Fixed to the experimental values of Ref. 8.

Although the TB model predicts the correct relative energetics of the phases, it is not capable of describing the subtle pressure-induced phase transformation $m \leftrightarrow o_I$. Figure 4 shows the common-tangent between the m and the o_{II} phases. As the pressure is increased, the model misses the correct sequence of the phases, predicting a $m \leftrightarrow o_{II}$ pressure-induced phase transformation at 5 GPa.

B. Cubic versus tetragonal phases

1. Static calculations

The relationship between the cubic and the tetragonal phases is governed by a volume dependent double well in the potential energy. Since the FLAPW calculation of Jansen[54,29] who predicted it first, the double well has been confirmed by

TABLE III. Energy differences (mRy/ZrO_2) between the zirconia polymorphs and the c phase calculated at the minimized structural parameters of Tables II and IV. The experimental values are derived from enthalpy differences at the phase transition temperature.

		ΔU^{t-c}	ΔU^{m-c}	ΔU^{O_I-c}	$\Delta U^{O_{II}-c}$
Expt.	Ref. 43	−4.2	−8.8		
SC-TB		−3.0	−7.4	−3.6	2.8
NFP		−3.6	−7.7		
PW-PP	Ref. 32	−3.3	−7.5		
PW-PP	Ref. 33	−3.5	−8.2	−5.3	
PW-PP	Ref. 34	−1.5[a] −5.9[b]	−4.4[a] −13.9[b]		0.7[a] 7.3[b]

[a]LDA calculation.
[b]Perdew-Wang GGC calculation.

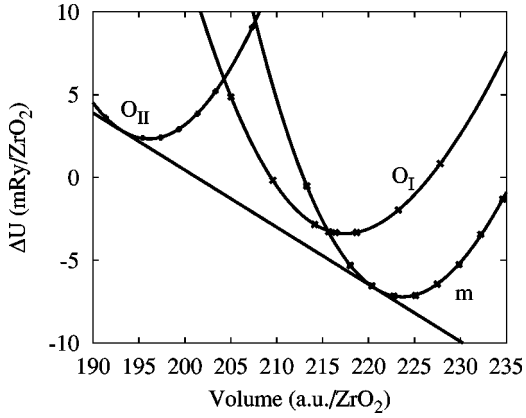

FIG. 4. Energy-volume curves for the monoclinic (m) and orthorhombic (o_I and o_{II}) phases calculated with the TB model.

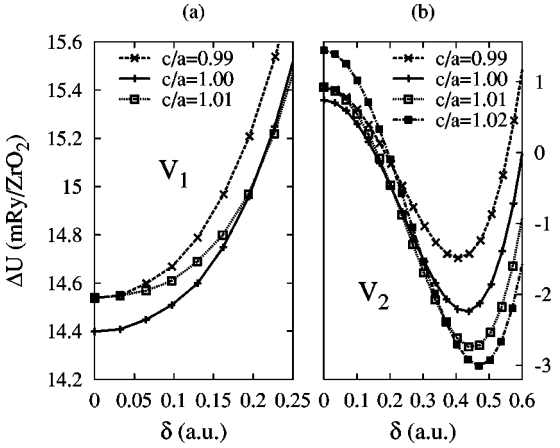

FIG. 5. SC-TB cohesive energy vs tetragonal distortion δ: volume and c/a dependence. (a) Single well at $V_1 = 198$ a.u/ZrO_2; (b) Double well at $V_2 = 218$ a.u/ZrO_2.

several other *ab initio* calculations and it is now well established.

In this section we analyze the nature of the 0 K energy surface by combining the information gained using two very different approaches: the NFP-LMTO method and the polarizable TB model. The qualitative and quantitative agreement between the results of the two calculations, shown in the previous section, entitles us to use the physical picture provided by the simpler model to interpret the *ab initio* results.

Starting from the c phase, the t structure can be obtained by continuously stretching the unit cell along the c crystallographic direction and by displacing the oxygen columns by δ along the tetragonal axis according to the X_2^- mode of vibration (Fig. 1). We calculated the total energy of the crystal using the two methods, for different values of (δ, c/a) at several volumes.

The energy curve exhibits a single-well or a double-well structure depending on the specific volume. At small volumes, V_1, the tetragonal distortion is energetically unfavored and the equilibrium structure is cubic (Fig. 5). When the cubic phase is stable, there is no distinct metastable tetragonal phase with which to compare its energy, so the energies of the two phases merge. At larger volumes, V_2, a structural instability appears and the c structure spontaneously distorts to the t one (Fig. 5).

The curvature of the energy surfaces is related to the phase transition mechanism. It is clear from Fig. 5 that $\partial^2 E/\partial(c/a)^2$ is positive, while $\partial^2 E/\partial\delta^2$ is negative: this suggests that the phase transition is driven by the δ instability and that the adjustment of the c/a ratio is a secondary effect. The coupling between these two order parameters will be further discussed when we interpret the double well using Landau theory.

Our local-density approximation (LDA) and TB results for the depth of the double well at the t-phase equilibrium volume, V_2, are consistent with the recent LDA values of ≈ 7 mRy.[33,34] This energy barrier for the 6-atom unit cell corresponds to a temperature of ≈ 1100 K. The same result

TABLE IV. External and internal degrees of freedom of the orthorhombic structures. Lattice parameters a, b, c in a.u., volumes in a.u./ZrO_2. The fractional coordinates of the non-equivalent sites are denoted with x, y, and z.

		Ortho I			*Ortho II*	
	Expt. Ref. 52	SC-TB This work	PW-PP Ref. 33	Expt. Ref. 53	SC-TB This work	PW-PP Ref. 34
Vol.	228.159	218.69	226.7	203.54	196.08	212.44
a	19.060	18.737	19.060 [a]	10.558	10.541	10.721
b/a	0.522	0.520	0.522[a]	0.596	0.592	0.593
c/a	0.505	0.511	0.505[a]	1.161	1.139	1.163
x_{Zr}	0.884	0.880	0.884	0.246	0.255	0.253
y_{Zr}	0.033	0.002	0.036	0.250	0.250	0.250
z_{Zr}	0.256	0.256	0.253	0.110	0.099	0.111
x_{O_1}	0.978	0.978	0.978	0.360	0.354	0.360
y_{O_1}	0.748	0.745	0.739	0.250	0.251	0.250
z_{O_1}	0.495	0.509	0.499	0.424	0.421	0.425
x_{O_2}	0.791	0.784	0.790	0.025	0.022	0.023
y_{O_2}	0.371	0.371	0.374	0.750	0.749	0.750
z_{O_2}	0.131	0.130	0.127	0.339	0.338	0.340

[a]Fixed to the experimental values of Ref. 52.

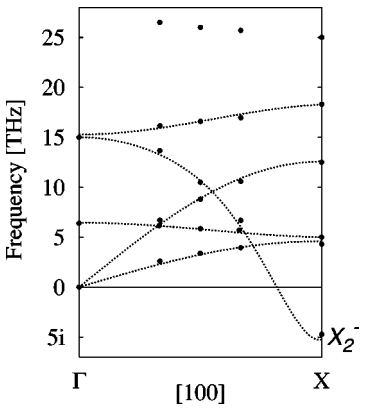

FIG. 6. Phonon dispersion curves of cubic zirconia in the [100] direction. Closed circles are TB calculations, dashed lines are guides to the eye. Note the imaginary frequency of the X_2^- mode of vibration.

was obtained by Jansen[54] with the FLAPW method who proposed a value of ≈ 1200 K. It is natural that these temperatures, extrapolated from the 0 K potential energy, underestimate the experimental phase transition temperature of 2570 K.[6] The experimentally observed phase transition temperature can be considered as the sum of the kinetic contributions of all the activated eigenmodes, while the calculated energy barrier refers to the kinetic contribution of the X_2^- eigenmode only. Even though it is reasonable to expect that at the phase transition the soft mode in the phonon spectra (Fig. 6) will be highly weighted in the total density of states, the kinetic energy kT associated with all the other modes of vibrations will still contribute to the measured phase transition temperature.

2. Physical interpretation of the double well

What causes the $c \leftrightarrow t$ symmetry breaking? The tetragonal distortion of the oxygen sublattice implies the following geometrical changes: (i) Two Zr-O bond lengths get smaller and two get longer but the average Zr-O distance increases. (ii) entire columns of oxygen atoms shift one with respect to each other (see Fig. 1) therefore the nearest-neighbor O-O distances along the column remain constant while the other four nearest-neighbor O-O distances increase. (iii) All the Zr-Zr distances remain constant. The overall increase of both the Zr-O and the O-O bond lengths is the basis of our interpretation of the double well, founded mainly on electrostatic arguments.

By adjusting the various parameters describing ionicity, covalency, and polarizability of the TB model we can select and isolate the effects that induce the double well, but before doing so it is instructive to understand how a simple RIM answers to the same question. It has been shown[20] that it is possible to reproduce the double well with a RIM in which there are two contributions: a repulsive short-ranged pairwise interaction U^{pair} and a long-ranged electrostatic term U^{ii}.

$$U^{\text{RIM}} = \sum_{i<j} A e^{-b r_{ij}} + \sum_{i<j} \frac{z_i z_j}{r_{ij}} = U^{\text{pair}} + U^{ii}, \qquad (16)$$

z is the ionic charge and r_{ij} is the interatomic distance between the ions i and j.

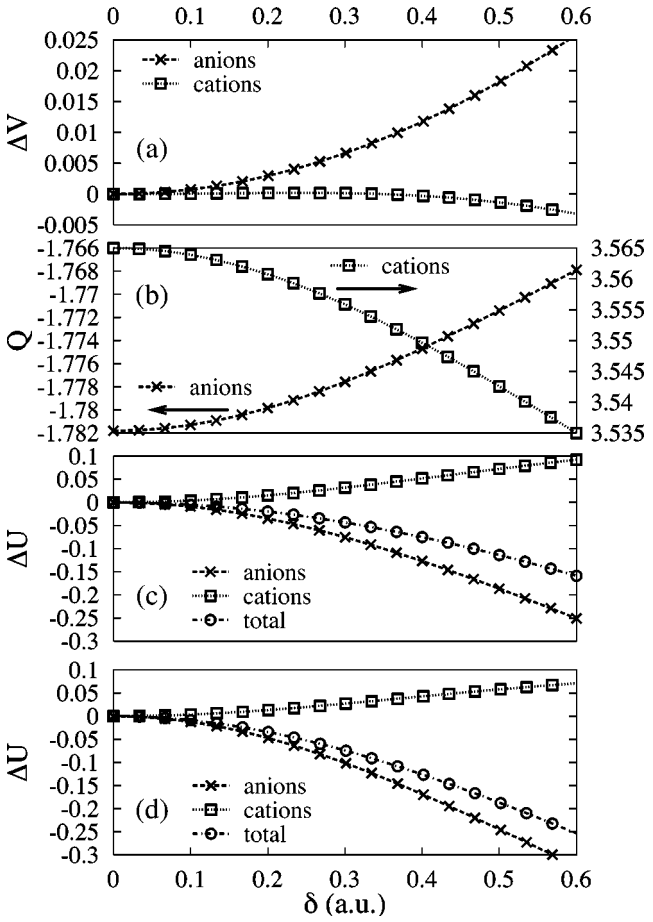

FIG. 7. δ dependence of: (a) Madelung potential, (b) self-consistent charge $Q = Q^e + Q^i$, (c) Electrostatic and Hubbard energies as in Eq. (17), (d) the same including dipoles and quadrupoles. The zero of energy is the top of the double well at V_2, total energies are in Ry/formula unit, other quantities in a.u./ion.

The Zr-O bonds increase and decrease in length in a symmetric way. As a net result, the centrosymmetric position of the oxygen atoms is a relative maximum of the Coulomb energy U^{ii}. The change in the Madelung potential caused by the tetragonal distortion is shown in Fig. 7(a). The overall increase of the O-Zr and O-O distances makes the oxygen sites much more sensitive to the change of the Madelung potential than the zirconium ones. The structural instability can therefore be interpreted as an effective way of minimizing the electrostatic energy of the oxygen sublattice. The repulsive Zr-O interaction counteracts the structural instability driven by the electrostatics, in a way which dominates at large displacements because of the exponential distance dependence of this repulsion. The double well shape of the energy profile is due to the different functional form of these opposing energy terms of Eq. (16). This argument clearly depends on the strength of the repulsion, and does not work if the repulsion is too weak.

It can be noticed that analogous terms are present in the TB model and a similar interpretation is tempting. However, we now have the additional effects due to polarization, covalency, and charge redistribution. Figure 7(b) shows that the absolute value of the self-consistent equilibrium charge Q decreases on both species. Consequently, in this approximation, the on-site energy

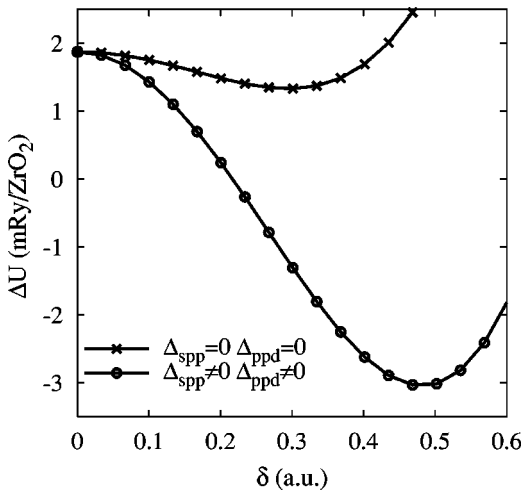

FIG. 8. Double well in the TB total energy at V_2: ($\times$) no coupling between the potential and the oxygen atomic orbitals; ($\bigcirc$) with dipoles and quadrupoles on the oxygen atoms.

$$\frac{1}{2}\sum_{\mathbf{R}L}\left[U\delta N_{\mathbf{R}l}^2+Q_{\mathbf{R}L}V_{\mathbf{R}L}\right], \tag{17}$$

plotted in Fig. 7(c), decreases not only because of the previous geometric arguments but also because the charge redistribution reduces the ionic charges and therefore both the O-O and Zr-Zr electrostatic interactions.

It is interesting to note that, on the oxygen atoms, the self-consistent charge $|Q^e|$ decreases with δ even though the total on-site potential, the sum of the Hubbard and electrostatic terms as in Eq. (17), increases. This nonintuitive behavior of the charge transfer is due to covalency. The charge transfer is controlled both by the on-site potential and by the bonding integrals, which depend on the Zr-O distance. For $\delta\neq 0$, the overall increase in the Zr-O distance results in a decrease in the magnitude of the hopping integrals, and this overcomes the opposing effect of change in the on-site potential, *pushing back* some electrons from the oxygen to the zirconium sites.

In the CIM-DQ, it was the quadrupole polarization of the O ions, which stabilized the tetragonal structure, so it is of interest to see if it is also the development of a quadrupole moment in the tetragonal phase, which stabilizes it within the SC-TB model.

In fact it turns out that covalency is the main effect, although polarizability is still significant. The *t* structure is stable with respect to the *c* one even with a *non*polarizable SC-TB model [Fig. 8 (top curve)]: the small energy difference is due to both ionicity and covalency of the crystal. The addition of the oxygen polarizability enhances the energy difference between the two phases deepening and broadening the double well [Fig. 8 (bottom curve)].

We can be more specific about the nature of the polarization. In the *c* structure, the first nonzero components of the electrostatic potential are V_0 and V_3. The latter could, in principle, induce an octapole moment Q_3 on the anions. We truncated the multipolar expansion of the atomic multipole moments to the quadrupoles Q_2, therefore, within this approximation, the ions in the *c* structure are not polarized. Higher-order terms can be included in the expansion, but the overall agreement of the results with both experiments and first-principle calculations demonstrates that the model is already capturing the important physics of the system.

As the anion sublattice is distorted, the symmetry lowering induces the $l=1$ and $l=2$ components of the potential, which couple the *s* and *p* oxygen atomic orbitals. The magnitude of the coupling, and therefore of the multipole moments, is controlled by the parameters Δ_{spp} and Δ_{ppd}. The latter, fixed in order to reproduce the electronic structure of the rutile phase, produces very weak quadrupole moments, whose contribution to the double well is negligible. The former controls the size of the dipole moments whose symmetric distribution further minimizes the electrostatic energy [Fig. 7(d)]. The total effect on the double well is shown in Fig. 8.

3. Landau theory

The $c\leftrightarrow t$ phase transition can be interpreted in terms of the Landau theory.[55] In a subsequent paper we plan to explore the free energy surface at $T>0$ with this formalism, so it is convenient to introduce it here to discuss the $T=0$ results. Experimentally, the mechanism of this phase transition has been very controversial and a clear description is still missing.[56–63]

Chan[64] suggested that a partial softening of an elastic constant is the driving force of this phase transition and, after symmetry considerations based on the elastic strains only, concluded that the phase transition must be of first order. We show here that the inclusion of the order parameter δ gives a second-order phase transition. A similar discussion has been given by Ishibashi and Dvořák.[65]

According to the Landau theory, the appropriate thermodynamic potential, which describes the relationship between the two phases of interest, is expanded in a Taylor series in one or more order parameters, in which the expansion coefficients are temperature dependent. The order parameters are nonzero in the low-symmetry phase and vanish in the high-symmetry one, providing therefore a unique way to differentiate the two phases. The terms involved in the Taylor expansion are invariants under the symmetry operations of the high-symmetry phase and can be identified using group theory.

In the case of zirconia, the *c* structure is unstable along the three crystallographic directions, therefore the distortions along *x*, *y*, and *z* have to be explicitly treated in the energy expansion. This suggests the following nine order parameters, defined in terms of the strain tensor $\boldsymbol{\epsilon}$, and grouped into four symmetry-adapted bases, which spans the corresponding irreducible representations:

$$\begin{aligned}
\delta_x,\delta_y,\delta_z &\qquad T_1\\
\epsilon_{xx}+\epsilon_{yy}+\epsilon_{zz} &\qquad A_1\\
(2\epsilon_{zz}-\epsilon_{xx}-\epsilon_{yy}),(\epsilon_{xx}-\epsilon_{yy})\sqrt{3} &\qquad E\\
\epsilon_{xy},\epsilon_{yz},\epsilon_{zx} &\qquad T_2.
\end{aligned}$$

A complete analysis involving all the order parameters will be done in a separate paper, here we simplify the total energy expansion selecting one of the three possible directions of the tetragonal axis. Under this hypothesis three order

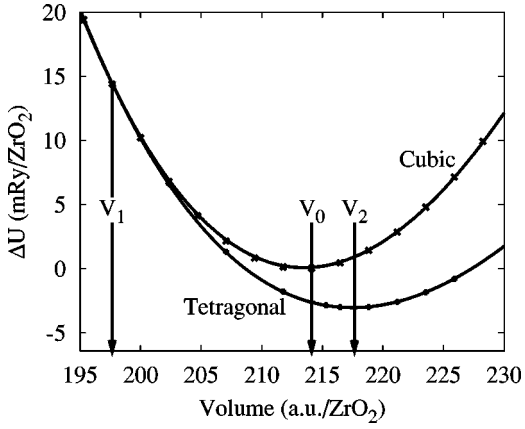

FIG. 9. Energy-volume curves for the c and t structures: note the convergence at small volumes V_1, V_0, and V_2 are the equilibrium volumes of the c and t phases, respectively.

parameters are necessary to describe the $c \leftrightarrow t$ phase transition of zirconia: δ, η, and η_0. The high-temperature c phase has the full cubic symmetry $m3m$ and the only degree of freedom is the hydrostatic strain $\eta_0 = \epsilon_{xx} + \epsilon_{yy} + \epsilon_{zz}$. The low-symmetry t phase is defined by the distortion of the anionic sublattice δ, which we define as the amplitude of the X_2^- mode of vibration, and by the tetragonal strain $\eta = (2\epsilon_{zz} - \epsilon_{xx} - \epsilon_{yy})$.

The three order parameters can be hierarchically classified according to the amount of symmetry breaking that they involve. The hydrostatic strain η_0 preserves the cubic symmetry of the crystal. The tetragonal strain η maintains the number of atoms in the primitive cell and lowers the symmetry to the point group $4/mmm$, which still has the mirror symmetry operation perpendicular to the tetragonal axis. The tetragonal distortion δ breaks this symmetry operation and involves cell doubling. Therefore, according to Landau theory, δ is the primary order parameter, η is the secondary, and η_0 is the tertiary one.

The potential energy is expanded as a power series in these order parameters around the equilibrium volume of the cubic phase V_0 (Fig. 9):

$$U - U^c_{V_0} = \frac{a_2}{2}\delta^2 + \frac{a_4}{4}\delta^4 + b_0\delta^2\eta_0 + b_1\delta^2\eta + \frac{c_0}{2}\eta_0^2 + \frac{c_1}{2}\eta^2 + \mathcal{O}(\delta^6). \tag{18}$$

The elastic constants c_0 and c_1 are proportional respectively to the bulk modulus and to $C' = \frac{1}{2}(c_{11} - c_{12})$ in the c phase described in the next section. The third-order term δ^3 is forbidden by symmetry, therefore this transition is of second order if a_2 goes negative.

The volume dependence of the order parameters can be studied by setting to zero $\nabla_\eta U$ and $\nabla_{\eta_0} U$. Both the *ab initio* and TB results (Fig. 10) confirm the analytic expressions:

$$\begin{cases} \eta = -\dfrac{b_1}{c_1}\delta^2 \\ \eta_0 = -\dfrac{b_0}{c_0}\delta^2 \end{cases} \Rightarrow \begin{cases} \delta \propto \sqrt{\eta_0} \\ \eta \propto \eta_0 . \end{cases} \tag{19}$$

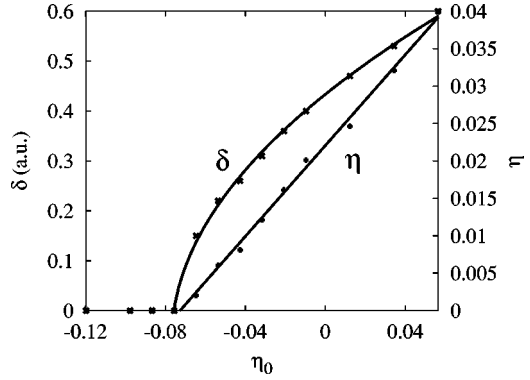

FIG. 10. Volume dependence of the order parameters calculated with the TB model: η_0 is the hydrostatic strain of the cubic cell from the reference volume V_0, η is the tetragonal strain of the cell, and δ (a.u.) is the tetragonal distortion of the oxygen sublattice.

These expressions show that the second-order strain terms of Eq. (18) are already proportional to δ^4 and therefore, within the chosen order of approximation, it is not necessary to include third-order terms in ϵ_{ij}. Moreover, from the static results it is clear that the description of the high-temperature stability of the c phase must go beyond the quasi-harmonic approximation. The higher the temperature, the larger the volume and, according to Fig. 10, the larger δ and η. Therefore, in a simple quasiharmonic picture, a higher temperature seems to favor the t phase with respect to c, in contradiction to the experimental observation.

The parameters c_1 and c_0 are known from the elastic properties of the crystal and have been calculated independently (see next section). The coefficients a_2 and a_4 have been fitted to the double well of an undistorted stress-free cubic crystal (in the sense $\eta = 0$ and $\eta_0 = 0$). In a similar way, b_1 and b_0 have been fitted to the double well of a tetragonal crystal at V_0 ($\eta_0 = 0$, $\eta \neq 0$) and of a cubic crystal near V_0 ($\eta = 0$, $\eta_0 \neq 0$), respectively. Figure 11(a) shows the three curves used for the fitting procedure. The agreement is very good even far away from the reference

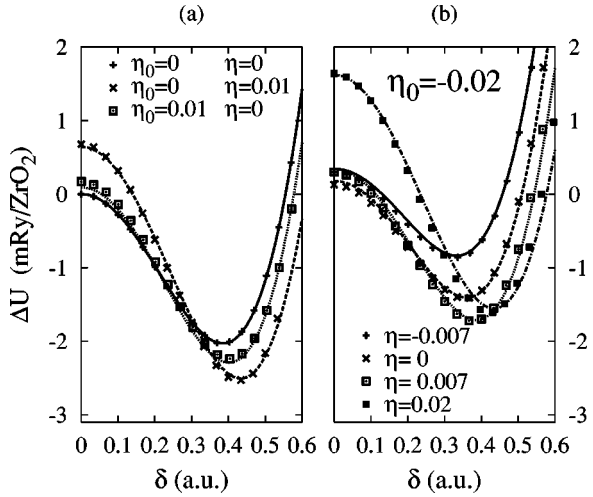

FIG. 11. SC-TB total energy vs tetragonal distortion δ. (a) Fit of the data with the Landau energy expansion Eq. (18); (b) transferability of the coefficients at values of hydrostatic (η_0) and tetragonal (η) strains different from the reference ones.

TABLE V. Coefficients (a.u.) of the energy Taylor expansion Eq. (18).

$a_2=-0.053$	$b_0=-0.062$	$c_0=0.621$
$a_4=0.347$	$b_1=-0.152$	$c_1=0.818$

volume of the energy expansion [Fig. 11(b)]. This demonstrates that the fourth-order truncation in Eq. (18) is sufficient to capture all the essential features of the 0 K energy surface.

Nardelli *et al.*[66,67] have shown the crucial role played by the coupling between different order parameters and how it can affect the correct interpretation of the phase transformation. To see this we substitute the relationships (19) back in Eq. (18):

$$U-U^c_{V_0}=\frac{a_2}{2}\delta^2+\left[\frac{a_4}{4}-\frac{b_0^2}{2c_0}-\frac{b_1^2}{2c_1}\right]\delta^4+\mathcal{O}(\delta^6). \quad (20)$$

The above equation shows that the coupling term $[(b_0^2/2c_0)+(b_1^2/2c_1)]$ can renormalize the fourth-order coefficient, and could make it negative. In that case it would be necessary to truncate Eq. (18) at the sixth-order term in δ, including therefore the third-order terms in the strain. These would then drive the phase transition making it first order.[64,68] The numerical values of the coefficients (Table V) allow us to estimate the amount of the coupling. We find that the coupling term is $\approx 20\%$ of $a_4/4$, not big enough to affect the sign of the fourth-order coefficient and therefore the 0 K calculations suggest that the phase transition is displacive of second order.

The temperature dependence of the elastic constants might change this description and the final answer will be given by high-temperature molecular dynamics calculations, which are in progress.

IV. DISTORTIONS

A. Elastic constants

The elasticity of *c* and *t* zirconia has been explored with the TB model. The analysis involved the distortion of the crystal along high-symmetry directions, the calculation of the total energy for different values of the distortion parameter and the fit of the results to a polynomial. The rigidity of the crystal with respect the particular distortion applied has been extracted from the quadratic coefficient of the energy series expansion. For each strain of the *t* structure, we constrained the volume to the predicted equilibrium value and minimized the energy with respect to the internal degrees of freedom.

Volume conserving stretches along the high-symmetry directions of the *c* unit cell $\langle 100\rangle$ and $\langle 111\rangle$ provide $C'=\frac{1}{2}(c_{11}-c_{12})$ and c_{44}, respectively. Extra distortions are necessary when the symmetry is lower: if *z* is the tetragonal axis, an independent set of five shear moduli were obtained by stretching along $\langle 100\rangle$, $\langle 001\rangle$, $\langle 111\rangle$, $\langle 110\rangle$, and $\langle 101\rangle$. The bulk moduli have been obtained by fitting the energy-volume curves with a Birch-Murnaghan equation of state.[69,70]

Liu *et al.*[71] used the slope of the acoustic branches at small wavelength of a ZrO_2-Y_2O_3 (15%) system to estimate the elastic constants of the cubic phase. Kandil *et al.*[72] directly measured the elastic constants of Yttria Stabilized Zirconia (YSZ) single crystals: the reference values included in Table VI are extrapolations to 0% impurities. To our knowledge there is no equivalent experimental study of the elasticity of the *t* phase. The most recent values[73] are measured via a powder diffraction technique on 12% Ce-doped *t* zirconia.

We compare our predictions with theoretical and experimental data in Table VI. The results of two other theoretical approaches, the Hartree-Fock and the PIB ones, are very different. As already mentioned in the Introduction, none of these calculations predicted the correct relative energetics of all the crystal structures. Elasticity is a property of the energy second derivative: a good description of the energy curves is a prerequisite for reliable elastic constant calculations.

The fairly good agreement of our calculations with the experiments further indicates that the SC-TB model captures the main physics of the bonding. The bulk modulus, however, is seriously overestimated: this may not be an intrinsic limitation of the TB model, because it was fit precisely to the NFP-LMTO calculation, which similarly overestimates this quantity.

TABLE VI. Elastic constants (GPa) of the *c* and *t* structures.

	SC-TB This work	Expt. Refs. 71, 72, 73	PIB Ref. 27	HF Ref. 30	DFT Ref. 33
			Cubic		
K_0	310	194 254	288	222	268
C'	175	167 165	195	304	
c_{44}	57	47 61	180	82	
			Tetragonal		
K_0	190	151	179		197
c_{11}	366	327	465		
c_{33}	286	264	326		
c_{12}	180	100	83		
c_{13}	80	62	49		
c_{44}	78	59	101		
c_{66}	88	64	156		

TABLE VII. Phonon frequencies (THz) at the Γ and X points of the BZ.

Mode	SC-TB This work	DFT Ref. 74	DFT Ref. 75	Expt. Refs. 68, 79, 80
			Γ point	
T_{1_u} (TO)	6.3	8.1	8.5	9.6
T_{2_g}	15.0	17.6	16.5	18.3
T_{1_u} (LO)		20.1	19.7	21.1
			X point	
X_2^-	5.1i	5.8i	5.9i	
X_5^-	4.5	4.9	3.5	5.1
X_5^+	5.0	8.9	11.7	
X_4^-	12.5	11.0	11.6	
X_4^+	18.1	17.0	16.0	
X_1^+	25.0	21.0	21.0	

B. Phonon spectra

In order to test the model further, as well as to give further insight into the spontaneous symmetry breaking of the c phase, we studied its vibrational properties. First-principle calculations[74,75] predict an imaginary frequency at the boundary of the Brillouin zone (BZ): this reinforces the idea that the phase transition is displacive, and driven by the softening of an optic mode.

Our calculations were carried out with the TB model on a 96-atom unit cell. The eigenvalues and eigenvectors of the possible vibrational modes in that unit cell, were found by diagonalizing the dynamical matrix, which we calculated using the direct method. The procedure was as follows.

Within the harmonic approximation, the potential energy Φ is expanded to second order in powers of the atomic displacements **u**:

$$\Phi=\Phi_0+\frac{1}{2}\sum_{\substack{l,\kappa,\alpha\\ l',\kappa',\beta}}\Phi_{\alpha\beta}\begin{pmatrix} ll'\\ \kappa\kappa'\end{pmatrix}u_\alpha\begin{pmatrix} l\\ \kappa\end{pmatrix}u_\beta\begin{pmatrix} l'\\ \kappa'\end{pmatrix}+\cdots. \tag{21}$$

We use the notation of Maradudin *et al.*:[76] κ and l label, respectively, the atom in the primitive cell and the position of the primitive cell with respect to some origin. The direct method consists in computing the force constants $\Phi_{\alpha\beta}$ via total energy and force calculations. In general, the atom κ in the l cell is displaced by a small amount in direction α and the Hellmann-Feynman forces on the other atoms are recorded. These give directly the quadratic terms in the total energy expansion. The force constants $\Phi_{\alpha\beta}$ can be related to the corresponding term of the dynamical matrix **D** via the usual relation:

$$D_{\alpha\beta}\begin{pmatrix}\mathbf{k}\\ \kappa\kappa'\end{pmatrix}=(1/\sqrt{M_\kappa M_{\kappa'}})\sum_l\Phi_{\alpha\beta}\begin{pmatrix} l\\ \kappa\kappa'\end{pmatrix}e^{-2\pi\mathbf{k}\cdot\mathbf{x}(l)}. \tag{22}$$

M_κ is the mass of the atom κ and **k** is a point in the BZ. The crystal symmetry can considerably reduce the number of necessary independent calculations.[77,78]

The phonon spectra plotted along the high-symmetry direction ⟨100⟩ are shown in Fig. 6. The main feature of the spectra is the imaginary frequency of the X_2^- mode of vibration, which corresponds to the tetragonal instability shown in Fig. 5. As already mentioned the tetragonal instability involves cell doubling therefore the corresponding eigenvector appears at the BZ border of the c phase. The soft mode at the X point is the natural consequence of the negative curvature of the energy surface at $\delta=0$ (Fig. 5). Setting to zero the dipolar polarizability of the anions ($\Delta_{spp}=0$), the X_2^- mode is still soft, $\nu=0.8i$, but the force constant corresponding to the instability is much smaller. This is consistent with Fig. 8 where the same effect is studied from the energetic point of view: the energy curve is concave at $\delta=0$ even when the oxygens are not polarizable.

The effect of the oxygen polarizability is evident on the T_{1u} infrared-active mode, which involves the rigid displacement of the two atomic sublattices. The calculated vibration frequency is 7.9 THz when the anions are not polarizable and 6.3 THz when the dipolar degree of freedom is allowed. The closer agreement of the nonpolarizable result with the DFT frequencies of 8.1–8.5 THz, together with the overestimation of the bulk modulus suggests that the present model could slightly overestimate both the short-range repulsion between closed shells of electrons, responsible for the high bulk modulus, and the long-range polarization effects, which make the T_{1u} frequency lower than the *ab initio* values. The results might be improved with a more accurate reparametrization but the physical interpretation of the *ab initio* results, which is the main objective of this analysis, is unlikely to change.

Table VII shows the general agreement of the TB model with other calculations and with the experimental data. The latter are measured by Raman spectroscopy and inelastic neutron scattering at high temperatures on YSZ.

Certain nonanalytical terms in the dynamical matrix have been neglected, namely those relating to macroscopic polarization or the Berry phase. For this reason our calculations cannot reproduce the LO-TO splitting of 12 THz calculated by Detraux *et al.*[74] The non-analytical terms can be approximated by knowing the Born effective charge and the dielectric tensor, both of which could in principle be obtained from our model. This has previously been done in a TB framework,[81] although not for ZrO_2, and we plan to investigate the effect in the future.

V. CONCLUSIONS

We have explored the predictive power of a polarizable SC-TB model by investigating the crystal stability of pure zirconia. The results of this extended TB model are in overall good agreement with our own *ab initio* (NFP-LMTO) calculations and with previous experimental and theoretical *ab initio* studies. This semiempirical model has captured the basic physics of the relative phase stability of zirconia with a set of parameters that are transferable between the crystal structures. A noteworthy improvement over all previous models is the absolute stability of the monoclinic structure at 0 K with respect to the usual set of alternatives. This demonstrates that the model is ready to deal with more complicated crystalline environments such as solid solutions, high-temperature distortions, or interfaces.

The TB model predicts that the covalent character of the Zr-O bond plays a major role in the energetics of zirconia, more so than the polarizability of the oxygen ions. For example, the double well about the cubic structure, absent in a rigid ion model, exists when covalency is included; it is further enhanced by including also polarizability at the dipole level. We do not believe that the separation between covalent effects and polarizability effects is unique, since it depends on the choice of basis functions. Quite possibly the previous polarizable ion models were capturing some effects of charge redistribution, which could alternatively be described by covalency. It remains to be seen if a model for zirconia without explicit covalency could satisfactorily reproduce all the structural energies.

The Landau theory, used to interpret the TB and *ab initio* results, together with the lattice dynamic analysis, shows that the $c \leftrightarrow t$ phase transition is displacive of the second order and is driven by the softening of the X_2^- mode of vibration. If it had been driven by a softening of the corresponding elastic constant $c_{11}-c_{12}$ it would have been a first-order transition. The partial softening of the elastic constants due to the temperature could also in principle change the character of the phase transition. We are currently applying the molecular dynamics technique to understand the high-temperature thermodynamic stability of the *c* phase and to explore the character of the phase transition. To this end we can use thermodynamic integration to go beyond the harmonic approximation. The preliminary results of these calculations will appear in the near future.[82]

Since the valence electrons are treated explicitly within the SC-TB model we also hope to be able to study the effects of point defects. This would be more difficult with a classical polarizable ion model because of the problems associated with charge conservation and redistribution.

ACKNOWLEDGMENTS

S.F. is grateful for support from the European Science Foundation, Forbairt, and the British Council, and for discussions with John Corish and Nigel Marks. A.T.P. and M.W.F. are grateful to the EPSRC for funding under Grants No. L66908 and No. L08380. This work has been supported by the European Communities HCM Network ''Electronic Structure Calculations of Materials Properties and Processes for Industry and Basic Science'' under Grant No. ERBFMRXCT980178.

[1] *Science and Technology of Zirconia*, edited by A. H. Heuer and L. W. Hobbs, Advances in Ceramics Vol. 3 (The American Ceramic Society, Columbus, OH, 1981).
[2] *Science and Technology of Zirconia II*, edited by N. Claussen, M. Rühle, and A. H. Heuer, Advances in Ceramics Vol. 12 (The American Ceramic Society, Columbus, OH, 1984).
[3] C. F. Grain, J. Am. Ceram. Soc. **50**, 288 (1967).
[4] M. G. Scott, J. Mater. Sci. **10**, 1527 (1975).
[5] V. S. Stubican and J. R. Hellman, in *Science and Technology of Zirconia* (Ref. 1), p. 25.
[6] P. Aldebert and J. P. Traverse, J. Am. Ceram. Soc. **68**, 34 (1985).
[7] R. J. Ackermann, S. P. Garg, and E. G. Rauth, J. Am. Ceram. Soc. **60**, 341 (1977).
[8] C. J. Howard, R. J. Hill, and B. E. Reichert, Acta Crystallogr., Sect. B: Struct. Sci. **B44**, 116 (1988).
[9] G. Teufer, Acta Crystallogr. **15**, 1187 (1962).
[10] J. Adam and M. D. Rogers, Acta Crystallogr. **12**, 951 (1959).
[11] J. D. McCullough and K. N. Trueblood, Acta Crystallogr. **12**, 507 (1959).
[12] D. K. Smith and H. W. Newkirk, Acta Crystallogr. **18**, 983 (1965).
[13] W. D. Kingery, *Introduction to Ceramics* (Wiley, New York, 1960).
[14] A. Dwivedi and A. N. Cormack, Philos. Mag. A **61**, 1 (1990).
[15] A. P. Mirgorodsky, M. B. Smirnov, and P. E. Quintard, Phys. Rev. B **55**, 19 (1997).
[16] A. Cormack and S. C. Parker, J. Am. Ceram. Soc. **73**, 3220 (1990).
[17] X. Li and B. Hafskjold, J. Phys.: Condens. Matter **7**, 1255 (1995).
[18] F. Shimojo, T. Okabe, F. Tachibana, M. Kobayashi, and H. Okazaki, J. Phys. Soc. Jpn. **61**, 2848 (1992).
[19] F. Shimojo and H. Okazaki, J. Phys. Soc. Jpn. **61**, 4106 (1992).
[20] M. Wilson, U. Schönberger, and M. W. Finnis, Phys. Rev. B **54**, 9147 (1996).
[21] S. Fabris, Master's thesis, University of Trieste, 1997.
[22] S. M. Ho, Mater. Sci. Eng. **54**, 23 (1982).
[23] M. W. Finnis, A. T. Paxton, M. Methfessel, and M. van Schilfgaarde, in *Tight Binding Approaches to Computational Materials Science*, edited by P. Turchi, A. Gonis, and L. Colombo, MRS Symposia Proceedings No. 491 (Materials Research Society, Pittsburgh, 1997).
[24] M. W. Finnis, A. T. Paxton, M. Methfessel, and M. van Schilfgaarde, Phys. Rev. Lett. **81**, 5149 (1998).
[25] P. K. Schelling, N. Yu, and J. W. Halley, Phys. Rev. B **58**, 1279 (1998).
[26] L. L. Boyer and B. M. Klein, J. Am. Ceram. Soc. **68**, 278 (1985).
[27] R. E. Cohen, M. J. Mehl, and L. L. Boyer, Physica B **150**, 1 (1988).
[28] F. Zandiehnadem and R. A. Murray, Physica B **150**, 19 (1988).
[29] H. J. Jansen, Phys. Rev. B **43**, 7267 (1991).
[30] R. Orlando, C. Pisani, C. Roetti, and E. Stefanovich, Phys. Rev. B **45**, 592 (1992).

[31] E. V. Stefanovich, A. L. Shluger, and C. R. A. Catlow, Phys. Rev. B **49**, 11 560 (1994).
[32] B. Králik, E. K. Chang, and S. G. Louie, Phys. Rev. B **43**, 7027 (1998).
[33] G. Stapper, M. Bernasconi, N. Nicoloso, and M. Parrinello, Phys. Rev. B **59**, 797 (1999).
[34] G. Jomard, T. Petit, A. Pasturel, L. Magaud, G. Kresse, and J. Hafner, Phys. Rev. B **59**, 4044 (1999).
[35] J. A. Majewski and P. Vogl, Phys. Rev. Lett. **57**, 1366 (1986).
[36] J. A. Majewski and P. Vogl, Phys. Rev. B **35**, 9666 (1987).
[37] A. J. Stone, *The Theory of Intermolecular Forces* (Clarendon Press, Oxford, 1996).
[38] O. Andersen, in *The Electronic Structure of Complex Systems*, Vol. 113 of *NATO Advanced Study Institute, Series B: Physics*, edited by P. Phariseau and W. Temmerman (Plenum, New York, 1984), p. 11.
[39] W. Foulkes and R. Haydock, Phys. Rev. B **39**, 12 520 (1989).
[40] A. P. Sutton, M. W. Finnis, D. G. Pettifor, and Y. Ohta, J. Phys. C **21**, 35 (1988).
[41] L. Goodwin, A. J. Skinner, and D. G. Pettifor, Europhys. Lett. **9**, 701 (1989).
[42] A. M. Stoneham, *Theory of Defects in Solids* (Clarendon Press, Oxford, 1975).
[43] R. J. Ackermann, E. G. Rauth, and C. A. Alexander, High. Temp. Sci. **7**, 304 (1975).
[44] Y. Kudoh, H. Takeda, and H. Arashi, Phys. Chem. Miner. **13**, 233 (1986).
[45] R. Suyama, T. Ashida, and S. Kume, J. Am. Ceram. Soc. **68**, C314 (1985).
[46] O. Ohtaka and S. Kume, J. Am. Ceram. Soc. **73**, 744 (1990).
[47] C. J. Howard, E. H. Kisi, and O. Ohtaka, J. Am. Ceram. Soc. **74**, 2321 (1991).
[48] L. G. Liu, J. Phys. Chem. Solids **41**, 331 (1980).
[49] S. Block, J. A. Jornada, and G. J. Piermarini, J. Am. Ceram. Soc. **85**, 497 (1985).
[50] O. Ohtaka, T. Yamanaka, S. Kume, E. Ito, and A. Navrotsky, J. Am. Ceram. Soc. **74**, 505 (1991).
[51] L. C. Ming and M. H. Manghnani, in *Solid-State Physics Under Pressure* (KTK Scientific, Tokyo, 1985), p. 135.
[52] O. Ohtaka, T. Yamanaka, S. Kume, N. Hara, H. Asano, and F. Izumi, Proc. Jpn. Acad., Ser. B: Phys. Biol. Sci. **66**, 193 (1990).
[53] J. Haines, J. M. Léger, S. Hull, J. P. Petitet, A. S. Pereira, C. A. Perottori, and J. A. H. de Jornada, J. Am. Ceram. Soc. **80**, 1910 (1997).
[54] H. J. Jansen and J. A. Gardner, Physica B **150**, 10 (1988).
[55] L. Landau and E. Lifshitz, *Statistical Physics* (Pergamon Press, Oxford, 1980), Vol. 5, Chap. XIV.
[56] I. Cohen and B. Schaner, J. Nucl. Mater. **9**, 18 (1963).
[57] T. Sakuma, Y. Yoshizawa, and H. Suto, J. Mater. Sci. **20**, 2399 (1985).
[58] A. Heuer and M. Rühle, in *Science and Technology of Zirconia II* (Ref. 2), p. 1.
[59] A. Heuer, R. Chaim, and V. Lanteri, Acta Metall. **35**, 661 (1987).
[60] V. S. Stubican, R. C. Hink, and S. P. Ray, J. Am. Ceram. Soc. **61**, 17 (1978).
[61] T. Sakuma, J. Mater. Sci. **22**, 4470 (1987).
[62] Y. Zhou, T. Lei, and T. Sakuma, J. Am. Ceram. Soc. **74**, 633 (1991).
[63] J. Katamura and T. Sakuma, J. Am. Ceram. Soc. **80**, 2685 (1997).
[64] S. K. Chan, Physica B **150**, 211 (1988).
[65] Y. Ishibashi and V. Dvoŕăk, J. Phys. Soc. Jpn. **58**, 4211 (1989).
[66] M. Buongiorno Nardelli and S. Baroni, Phys. Rev. Lett. **69**, 1069 (1992).
[67] M. Buongiorno Nardelli, S. Baroni, and P. Giannozzi, Phys. Rev. B **51**, 8060 (1995).
[68] P. W. Anderson and E. I. Blount, Phys. Rev. Lett. **14**, 217 (1965).
[69] F. D. Murnaghan, Proc. Natl. Acad. Sci. USA **30**, 244 (1944).
[70] F. Birch, J. Geophys. Res. **83**, 1257 (1978).
[71] D. W. Liu, C. H. Perry, A. A. Feinberg, and R. Currat, Phys. Rev. B **36**, 9212 (1987).
[72] H. M. Kandil, J. D. Greimer, and J. F. Smith, J. Am. Ceram. Soc. **67**, 341 (1982).
[73] E. H. Kisi and C. J. Howard, J. Am. Ceram. Soc. **81**, 1682 (1998).
[74] F. Detraux, Ph. Ghosez, and X. Gonze, Phys. Rev. Lett. **81**, 3297 (1998).
[75] K. Parlinski, Z. Q. Li, and Y. Kawazoe, Phys. Rev. Lett. **78**, 4063 (1997).
[76] A. A. Maradudin, E. W. Montroll, and G. H. Weiss, in *Solid State Physics, Advances in Research and Applications*, edited by F. Seitz and D. Turnbull (Academic Press, New York, 1963), p. 1.
[77] A. A. Maradudin and S. H. Vosko, Rev. Mod. Phys. **40**, 1 (1968).
[78] J. L. Warren, Rev. Mod. Phys. **40**, 38 (1968).
[79] D. W. Liu, Ph.D. thesis, Northeastern University, 1984.
[80] J. Cai, C. Raptis, Y. S. Raptis, and E. Anastassakis, Phys. Rev. B **51**, 201 (1995).
[81] J. Bennetto and D. Vanderbilt, Phys. Rev. B **53**, 15 417 (1996).
[82] S. Fabris, A. T. Paxton, and M. W. Finnis (unpublished).